JACS
JOURNAL OF THE AMERICAN CHEMICAL SOCIETY

ARTICLE

pubs.acs.org/JACS

Influence of Thiolate Ligands on Reductive N−O Bond Activation. Probing the O_2^- Binding Site of a Biomimetic Superoxide Reductase Analogue and Examining the Proton-Dependent Reduction of Nitrite

Gloria Villar-Acevedo, Elaine Nam, Sarah Fitch, Jason Benedict, John Freudenthal, Werner Kaminsky, and Julie A. Kovacs*

Department of Chemistry, University of Washington, Seattle, Washington 98195, United States

Supporting Information

ABSTRACT: Nitric oxide (NO) is frequently used to probe the substrate-binding site of "spectroscopically silent" non-heme Fe^{2+} sites of metalloenzymes, such as superoxide reductase (SOR). Herein we use NO to probe the superoxide binding site of our thiolate-ligated biomimetic SOR model $[Fe^{II}(S^{Me_2}N_4(tren))]^+$ (**1**). Like NO-bound *trans*-cysteinate-ligated SOR (SOR-NO), the rhombic $S = 3/2$ EPR signal of NO-bound *cis*-thiolate-ligated $[Fe(S^{Me_2}N_4(tren)(NO)]^+$ (**2**; $g = 4.44, 3.54, 1.97$), the isotopically sensitive $\nu_{NO}(\nu_{15}NO)$ stretching frequency ($1685(1640)\ cm^{-1}$), and the 0.05 Å decrease in Fe−S bond length are shown to be consistent with *the oxidative addition of NO to Fe(II)* to afford an $Fe(III)-NO^-$ $\{FeNO\}^7$ species containing high-spin ($S = 5/2$) Fe(III) antiferromagnetically coupled to NO^- ($S = 1$). The *cis* versus *trans* positioning of the thiolate does not appear to influence these properties. Although it has yet to be crystallographically characterized, SOR-NO is presumed to possess a bent Fe−NO similar to that of **2** (Fe−N−O = 151.7(4)°). *The N−O bond is shown to be more activated in* **2** relative to N- and O-ligated $\{FeNO\}^7$ complexes, and this is *attributed to the electron-donating properties of the thiolate ligand.* Hydrogen-bonding to the cysteinate sulfur attenuates N−O bond activation in SOR, as shown by its higher ν_{NO} frequency ($1721\ cm^{-1}$). In contrast, the ν_{O-O} frequency of the SOR peroxo intermediate and its analogues is not affected by H-bonds to the cysteinate sulfur or other factors influencing the Fe−SR bond strength; these only influence the ν_{Fe-O} frequency. Reactions between **1** and NO_2^- are shown to result in the *proton-dependent heterolytic cleavage of an N−O bond.* The mechanism of this reaction is proposed to involve both $Fe^{II}-NO_2^-$ and $\{FeNO\}^6$ intermediates similar to those implicated in the mechanism of NiR-promoted NO_2^- reduction.

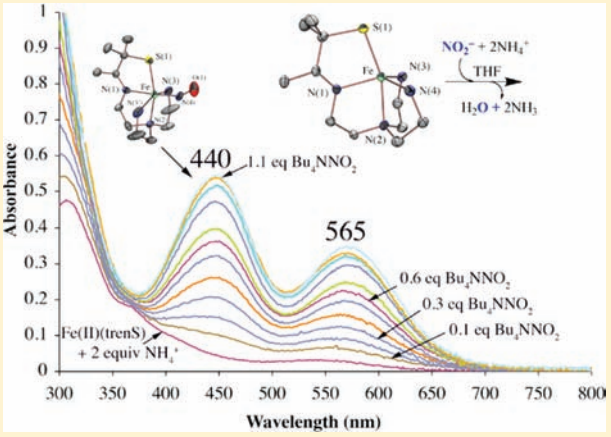

INTRODUCTION

Superoxide reductases (SORs) are cysteinate-ligated non-heme iron enzymes that selectively reduce superoxide (O_2^-) to hydrogen peroxide (H_2O_2) via a putative Fe(III)−OOH intermediate. Synthetic analogues of this peroxo intermediate have been reported by several groups.[1−6] Exogenous ligands, such as azide, nitric oxide, and cyanide, have been shown to bind to the high-spin ($S = 2$) N_4SFe^{2+} SOR site,[4] *trans* to an apical cysteine,[7] consistent with an inner-sphere mechanism of superoxide reduction. Detailed spectroscopic data are available for NO-bound SOR (SOR-NO);[8] however, this form of the enzyme has yet to be crystallographically characterized. Five-coordinate, thiolate-ligated $[Fe^{II}(S^{Me_2}N_4(tren))]^+$ (**1**)[9] was shown previously by our group to reduce superoxide (O_2^-) via a metastable hydroperoxo intermediate $[Fe^{III}(S^{Me_2}N_4(tren)-(OOH)]^+$—the first reported example of a synthetic thiolate-ligated iron-peroxo.[1] This biomimetic SOR analogue also reacts with dioxygen (O_2)[10] to afford a metastable intermediate that converts to μ-oxo dimer $[Fe^{III}(S^{Me_2}N_4(tren))]_2(\mu^2\text{-}O)(PF_6)_2$ upon warming.[10] Given the architecture of our $(tren)N_4{}^{Me_2}S^-$ ligand, O_2 and O_2^- are assumed to bind *cis* with respect to the thiolate; however, in the absence of crystallographic evidence, this is difficult to prove. Nitric oxide is frequently used to probe O_2 binding sites[8,11−14] and form analogues of key metastable $Fe-O_2$ intermediates, since its reduced derivative (NO^-) is isoelectronic with O_2 but affords a more stable, highly covalent Fe−NO bond.[15] Since it is a radical, NO is also frequently used as a tag to probe "spectroscopically silent" Fe^{2+} enzyme substrate-binding sites such as those of isopenicillin N-synthase (IPNS)[14,16] and superoxide reductase (SOR).[8] The substrate-derived thiolate ligand of the IPNS iron active site has been shown to stabilize both the key $Fe-O_2^-$ superoxo intermediate and the Fe−NO derivative.[16] The thiolate ligand of the

Received: August 31, 2010
Published: January 5, 2011

   dx.doi.org/10.1021/ja107551u | *J. Am. Chem. Soc.* 2011, 133, 1419–1427

synthetic SOR peroxo intermediate analogue $[(L^8py_2)Fe(III)(SR)(OOR)]^+$ was shown to increase its lifetime,[4] whereas those of $[Fe(III)([15]aneN_4)SAr(OOR)]^+$ and $[Fe(III)(cyclam\text{-}PrS)(OOH)]^+$ were shown the weaken the Fe−OOR(H) bond without affecting the O−O bond.[2,3]

In order to gain insight regarding the mechanism of O_2^- reduction by our thiolate-ligated SOR analogue $[Fe^{II}(S^{Me_2}N_4(tren))]^+$ (**1**) and probe its superoxide and dioxygen binding site, we describe herein the synthesis, and geometric and electronic structure properties of a more stable NO-bound analogue. Comparison of the properties of this SOR-NO analogue with those of SOR-NO[17] should allow us to determine how the superoxide binding sites differ and whether this influences properties critical to promoting superoxide reduction. Upon binding to transition metals, the N−O bond of nitric oxide can, in some cases, be activated via π-back-donation into a π^*(NO) orbital.[18] Electron-rich thiolate ligands have also been shown to enhance N−O bond activation by donating electron density to a metal ion orbital that is involved in σ-overlap with a σ^*(NO) orbital.[8,19] A similar mechanism may be involved in the activation of thiolate-ligated peroxo O−O bonds. Thus, information regarding N−O bond strength dependence on the presence of thiolate donors and their *cis* vs *trans* orientation could provide insight regarding the influence of thiolates on peroxo bond cleavage. The ability of reduced **1** to activate and cleave the N−O bond of additional substrates such as NO_2^- will also be explored.

EXPERIMENTAL SECTION

General Methods. All reactions were performed under an atmosphere of dinitrogen in a glovebox, using standard Schlenk techniques, or using a custom-made solution cell equipped with a threaded glass connector sized to fit a dip probe. Reagents purchased from commercial vendors were of the highest purity available and used without further purification. 3-Methyl-3-mercapto-2-butanone[20] and $[Fe^{III}((S^{Me_2}N_5(tren)(MeCN)][BPh_4]_2$ (**8**)[1] were synthesized as previously described. The triflate salt of $[Fe^{II}(S^{Me_2}N_4(tren))](OTf)$ (**1**) was synthesized as previously described,[9] using NaOTf in place of $NaPF_6$. Toluene, tetrahydrofuran (THF), diethyl ether (Et_2O), acetonitrile (MeCN), and pentane were rigorously degassed and purified using solvent purification columns, housed in a custom stainless steel cabinet, and dispensed via a stainless steel Schlenk line (GlassContour). Methanol (MeOH) and ethanol (EtOH) were distilled from magnesium methoxide and degassed prior to use. Methylene chloride (DCM) was distilled from CaH_2 and degassed prior to use. ^{1}H NMR spectra were recorded on Bruker AV 300 or Bruker AV 301 FT-NMR spectrometers and are referenced to an external standard of TMS (paramagnetic compounds) or to residual protio solvent (diamagnetic compounds). Chemical shifts are reported in ppm, and coupling constants (J) are in Hz. EPR spectra were recorded on a Bruker EPX CW-EPR spectrometer operating at X-band frequency at ~7 K. IR spectra were recorded on a Perkin-Elmer 1700 FT-IR spectrometer as KBr pellets. Cyclic voltammograms were recorded in MeCN (100 mM $Bu^n_4N(PF_6)$ solutions) on a PAR 273 potentiostat utilizing a glassy carbon working electrode, a platinum auxiliary electrode, and an SCE reference electrode. Magnetic moments (solution state) were obtained using Evans's method[21] as modified for superconducting solenoids.[22] Temperatures were obtained using Van Geet's method.[23] Solid-state magnetic measurements were obtained with polycrystalline samples in gel-caps using a Quantum Design MPMS S5 SQUID magnetometer. Ambient-temperature electronic absorption spectra were recorded on a Hewlett-Packard model 8450 spectrometer, interfaced to an IBM PC. Low-temperature electronic absorption spectra were recorded using a Varian Cary 50 spectrophotometer equipped with a fiber optic cable connected to a "dip" ATR probe (C-technologies), with a custom-built two-neck solution sample holder equipped with a threaded glass connector (sized to fit the dip probe). Elemental analyses were performed by Galbraith Atlantic Microlabs, Norcross, GA.

Synthesis of $[Fe(S^{Me_2}N_4(tren)(NO)](OTf)$ (2). Reduced $[Fe^{II}(S^{Me_2}N_4(tren))](OTf)$ (**1**) (200 mg, 0.448 mmol) was dissolved in acetonitrile and placed in a thick-walled bomb, equipped with a Teflon stopcock and a side arm joint. On a high-vacuum line, the solution was frozen (by placing the flask in liquid nitrogen), and the container was evacuated. Nitric oxide gas (420 Torr, 1.2 equiv) (Scotts Specialty Gases) was then added to the frozen solution. The container was sealed, and the contents were allowed to thaw. The solution was stirred overnight under nitrogen and then concentrated under vacuum to ~5 mL. Pentane (5 mL) and Et_2O (25 mL) were layered on top of this solution, and the layers were allowed to diffuse together. After 2 days, a brown powder formed (159 mg, 70% yield). ESI-MS: calcd for $[FeC_{11}H_{25}N_5OS]^+$, 331.269; found, 331.2. Electronic absorption: in CH_3CN, λ_{max} (ϵ) = 440 (2560), nm; in MeOH, λ_{max} (ϵ) = 438 (2560) nm. IR (KBr pellet): ν (cm^{-1}) 1605 (imine), 1685 (ν_{NO}). Solution magnetic moment (303 K, MeCN): μ_{eff} = 4.12 μ_B, $E_{1/2}$(MeCN) = +450 mV vs SCE. EPR (MeCN/toluene glass (1:1), 7 K): g_1 = 4.41, g_2 = 3.60, g_3 = 1.98. Anal. Calcd for $FeC_{35}H_{43}BN_5O_1S_1$: C, 64.74; H, 6.62; N, 10.79. Found: C, 64.67; H, 6.53; N, 10.29.

Synthesis of $[Fe^{III}(S^{Me_2}N_4(tren))(NO_2)](PF_6)$ (7). Acetonitrile-bound[1] $[Fe^{III}(S^{Me_2}N_4(tren))MeCN](PF_6)_2$ (500 mg. 0.789 mmol) and n-Bu_4NNO_2 (227 mg, 0.789 mmol, Fluka) were dissolved in MeCN (25 mL) and allowed to stir for 24 h under a nitrogen atmosphere in a glovebox. The solution was filtered through a fine glass frit, MeCN was removed under reduced pressure, and the solution was concentrated to ~1 mL. Diethyl ether (25 mL) was then layered on top of the solution, and the two layers were allowed to diffuse together at −30 °C. After 24 h, a purple solid (356 mg. 92%) was isolated. ESI-MS: calcd for $[FeC_{11}H_{25}N_5O_2S]^+$, 348.26; found, 347.5. Electronic absorption spectrum: in MeOH, λ_{max} (ϵ) = 565 (1460) nm. IR (KBr pellet): ν (cm^{-1}) 1608 (imine), $\nu_{asym}(NO_2)$ = 1478 cm^{-1}, and $\nu_{sym}(NO_2)$ = 1362 cm^{-1}. Solution magnetic moment (303 K, MeCN): μ_{eff} = 1.76 μ_B, $E_{1/2}$(MeCN) = −0.480 V vs SCE. EPR (MeOH/EtOH glass (9:1), 7 K): g_1 = 2.17, g_2 =2.13, g_3 = 1.98. Anal. Calcd for $FeC_{11}H_{25}PN_5O_2F_6S$: C, 26.84; H, 5.12; N, 14.23. Found: C, 27.67; H, 5.53; N, 14.59.

Formation of $[Fe^{III}(S^{Me_2}N_4(tren))(NO_2)](BPh_4)$ (7) via O_2 Oxidation of $[Fe(S^{Me_2}N_4(tren)(NO)][BPh_4]$ (2). A solution of $[Fe(S^{Me_2}N_4(tren)(NO)][BPh_4]$ (200 mg, 0.308 mmol) in 30 mL of acetonitrile was stirred in air for 30 min and then stirred under N_2 for an additional 5 h. The solution was then filtered, concentrated to ~2 mL, layered with ~25 mL of ether, and placed at −30 °C . The two layers diffused together overnight to afford purple crystals (172 mg, 86%). ESI-MS: calcd for $[FeC_{11}H_{25}N_5O_2S]^+$, 348.26; found, 347.5. Electronic absorption: in CH_3CN, λ_{max} (ϵ) = 565 (1460) nm. IR (KBr pellet): ν (cm^{-1}) 1682 (imine), 1478 cm^{-1} (ν_{asym} (NO_2)), and 1362 cm^{-1} (ν_{sym}(No_2)). Solution magnetic moment (303 K, MeCN): μ_{eff} = 1.76 μ_B, $E_{1/2}$(MeCN) = −0.480 V vs SCE. EPR (MeOH/EtOH glass (9:1), 7 K): g_1 = 2.18, g_2 =2.14, g_3 = 1.99.

X-ray Crystallographic Structure Determination. A brown prism of **2** (0.26 × 0.24 × 0.14 mm (0.30 × 0.21 × 0.18 mm)) was mounted on a glass capillary with oil. Data were collected at −143 °C. The crystal-to-detector distance was set to 30 mm, and exposure time was 60 s per degree for all data sets with a scan width of 1.0°. The data collection was 99% complete to 25° in θ. A total of 34 240 partial and complete reflections were collected, covering the indices h = −19 to 18, k = −11 to 11, l = −20 to 20. A total of 2541 reflections were symmetry independent, and the R_{int} = 0.0599 indicated that the data were good (average quality = 0.07). Indexing and unit cell refinements indicated an orthorhombic P lattice in the space group *Pnma* (No. 62). The data were integrated and scaled using hkl-SCALEPACK, and an absorption

Table 1. Crystal Data, Intensity Collections,[a] and Structure Refinement Parameters for [Fe($S^{Me_2}N_4$(tren))(NO)](OTf) (2) and [Fe(III)($S^{Me_2}N_4$(tren))(NO_2)][PF_6] (7)

	2	7
formula	$FeC_{12}H_{25}F_3N_5O_4S_2$	$FeC_{11}H_{25}F_6N_5O_2PS$
MW	480.34	492.24
T, K	130(2)	130(2)
unit cell	orthorhombic	orthorhombic
a, Å	14.4552(2)	13.6260(5)
b, Å	8.5295(5)	8.5790(9)
c, Å	15.6713(4)	15.8870(10)
V, Å^3	1932.2(3)	1857.1(2)
Z	4	4
d(calc), g/cm^3	1.651	1.761
space group	*Pnma*	*Pnma*
R	0.0514[b]	0.0707[b]
R_w	0.1413[c]	0.1865[d]
GOF	1.025	1.018

[a] Mo Kα (λ = 0.7107 Å) radiation; graphite monochromator; −90 °C. [b] $R = \sum||F_o| - |F_c||/\sum|F_o|$. [c] $R_w = [\sum w(|F_o| - |F_c|)^2/\sum wF_o^2]^{1/2}$, where $w^{-1} = [\sigma^2_{count} + (0.05F^2)^2]/4F^2$. [d] $R_w = \{\sum[w(F_o^2 - F_c^2)^2]/\sum[w(F_o^2)^2]\}^{1/2}$; $w = 1/[\sigma^2(F_o^2) + (0.0620P)^2 + 0.000P]$, where $P = [F_o^2 + 2F_c^2]/3$.

correction was performed using SORTAV. Solution by direct methods (SIR97) produced a complete heavy-atom phasing model consistent with the proposed structure. All non-hydrogen atoms were refined anisotropically by full-matrix least-squares methods, while all hydrogen atoms were then located using a riding model. The structure showed disorder of the nitric oxide oxygen O(1) and one of the methylene groups in the amine/imine chelate ring (N(1)$(CH_2)_2$N(2)) with respect to a mirror plane containing N(1), N(4), Fe, and S(1).

A purple crystal plate of 7 (0.07 × 0.24 × 0.09 mm) was mounted on a glass capillary with oil. Data were collected at −143 °C. The crystal-to-detector distance was 30 mm, and exposure time was 30 s per degree for all sets. The scan width was 2.0°. Data collection was 92.7% complete to 27.09° and 97.4% complete to 25° in θ. A total of 26 490 partial and complete reflections were collected, covering the indices $h = -17$ to 17, $k = -10$ to 10, $l = -19$ to 19. A total of 2023 reflections were symmetry independent, and the R_{int} = 0.1474 indicated that the data were of less than average quality (0.07). Indexing and unit cell refinement indicated an orthorhombic P lattice in the space group *Pnma* (No.62). The data were integrated and scaled using hkl-SCALEPACK. Solution by direct methods (SIR97) produced a complete heavy-atom phasing model consistent with the proposed structure. All hydrogen atoms were located using a riding model. All non-hydrogen atoms were refined anisotropically by full-matrix least-squares. Crystal data for **2** and **7** are presented in Table 1. Selected bond distances and angles are assembled in the following section in Table 2.

RESULTS AND DISCUSSION

Reactivity of [$Fe^{II}(S^{Me_2}N_4$(tren))]$^+$ (1) with Nitric Oxide (NO). Quantitative addition of 1.0 equiv of NO(g) to an acetonitrile solution of five-coordinate, thiolate-ligated [$Fe^{II}(S^{Me_2}N_4$(tren))]$^+$ (**1**) under anaerobic (Scheme 1) conditions affords a compound with a parent ion in the triple quad ESI-MS (m/z = 330.7; Figure S-1, Supporting Information) that is consistent with the addition of 1 equiv of NO. Nitric oxide binding to **1** was confirmed by X-ray crystallography. As shown in the ORTEP diagram in Figure 1, nitric oxide binds *cis* to the thiolate sulfur and *trans* to the imine nitrogen

Table 2. Selected Bond Distances (Å) and Bond Angles (deg) for the Cations of [$Fe^{II}(S^{Me_2}N_4$(tren))]$^+$(PF_6) (1), [Fe($S^{Me_2}N_4$(tren))(NO)](OTf) (2), [$Fe^{III}(S^{Me_2}N_4$(tren))(OAc)](BPh_4) (3),[24] [$Fe^{III}(S^{Me_2}N_4$(tren))(N_3)](PF_6) (4),[24] and [$Fe^{III}(S^{Me_2}N_4$(tren)(NO_2)](PF_6) (7)

	1	2	3	4	7
Fe−S(1)	2.3281(9)	2.278(1)	2.168(2)	2.176(2)	2.177(3)
Fe−N(1)	2.091(3)	2.099(3)	1.910(6)	1.917(6)	1.951(9)
Fe−N(2)	2.268(3)	2.211(3)	2.050(6)	2.002(6)	2.053(8)
Fe−N(3)	2.131(3)	2.198(3)	2.003(6)	2.011(5)	2.036(6)[b]
Fe−N(4)	2.117(3)	2.198(3)	2.000(5)	2.002(5)	2.036(6)[b]
Fe−X[a]	N/A	1.770(3)	1.972(5)	1.999(6)	1.963(10)
N−O(1)	N/A	1.118(6)	N/A	N/A	1.218(13)
N−O(2)	N/A	N/A	N/A	N/A	1.171(13)
Fe−N−O	N/A	151.7(4)	N/A	N/A	123.9(9)
S(1)−Fe−N(1)	84.02(8)	82.57(8)	87.0(2)	86.8(2)	85.4(2)
S(1)−Fe−N(2)	163.02(7)	162.45(9)	172.1(2)	172.1(2)	170.0(3)
N(1)−Fe−X[a]	N/A	177.5(1)	174.9(2)	176.7(2)	176.3(4)
X−Fe−S(1)[a]	N/A	95.0(1)	94.96(16)	95.5(2)	90.9(3)
N(3)−Fe−N(4)	115.2(1)	154.3(1)	163.4(2)	165.6(2)	163.5(4)

[a] X = NO (**2**), NO_2^- (**7**), OAc^- (**3**), and N_3^- (**4**). [b] Because **2** and **7** each lie on a crystallographic mirror plane that relates N(3) and N(3′), there are only four, as opposed to five, symmetry-independent nitrogen atoms. For the purposes of comparison, N(3′) for structures **2** and **7** is listed as N(4) in this table, and the nitric oxide and nitrite nitrogens for structures **2** and **7** are listed as X.

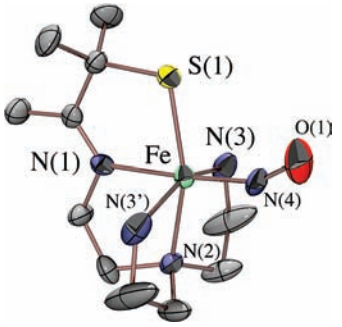

Figure 1. ORTEP plot of the cation of [Fe($S^{Me_2}N_4$(tren)(NO)][OTf] (**2**). All H-atoms have been omitted for clarity.

Scheme 1. Synthesis of [Fe($S^{Me_2}N_4$(tren)(NO)]$^+$ (2)

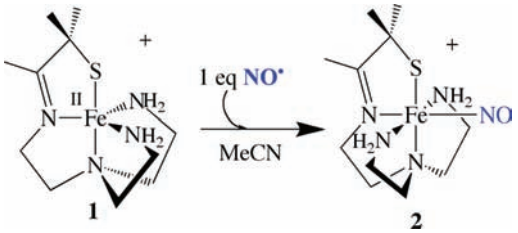

(N(1)). This *cis* orientation is similar to that of NO-bound IPNS[16] but contrasts with the presumed *trans* orientation in SOR-NO.[8] Selected bond distances (Å) and angles (deg) of [Fe($S^{Me_2}N_4$(tren)-(NO)]$^+$ (**2**) are compared with those of **1**, as well as previously reported [$Fe^{III}(S^{Me_2}N_4$(tren))(OAc)]$^+$ (**3**)[24] and [$Fe^{III}(S^{Me_2}N_4$-(tren))(N_3)]$^+$ (**4**),[24] in Table 2. As is true for the majority of

dx.doi.org/10.1021/ja107551u |*J. Am. Chem. Soc.* 2011, 133, 1419–1427

Scheme 2

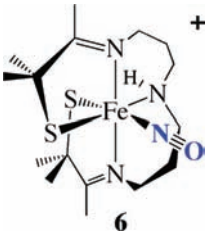

6

{FeNO}^{7} systems (*vide infra*),[11,18,25] the Fe−N(4)−O(1) bond angle of **2** is bent (151.7(4)°). This angle is also presumed to be bent in SOR-NO;[8] however, crystallographic data are not yet available to support this. In **2**, this angle is bent toward the *cis* thiolate sulfur (Figure 1), suggesting that if the hydroperoxo's orientation in $[Fe^{III}(S^{Me_2}N_4(tren)(OOH)]^+$ is the same, it would be capable of H-bonding to the sulfur. A hydrogen-bonded ring structure may, in fact, provide a driving force for the formation of hydroperoxide-ligated $[Fe^{III}(S^{Me_2}N_4(tren)(OOH)]^+$. Most significant in the structure of **2** is the fact that the Fe−S bond decreases in length upon NO binding (from 2.3281(9) Å in **1** to 2.278(1) Å in **2**), consistent with the *oxidative addition* of NO to the metal ion. This contrasts with the Fe−S bond lengthening (by 0.11 Å) that occurs upon NO binding to our previously reported ferric complex $[Fe^{III}(S_2{}^{Me_2}N_3(Pr,Pr))]^+$ (**5**),[26] to afford *trans*/*cis* bis-thiolate-ligated $[Fe(S_2{}^{Me_2}N_3(Pr,Pr))(NO)]^+$ (**6**, Scheme 2). As shown by the considerably shorter Fe−S distances in the ferric complexes **3** and **4** (Table 2),[24] NO binding to **1** induces only a fractional increase in oxidation state (*vide infra*).

With transition-metal nitric oxide complexes, the assignment of oxidation states is somewhat ambiguous due to the extensive delocalization of electrons within the highly covalent M−NO bond. For this reason, it is preferable to describe complexes of this type using the Enemark and Feltham notation {MNO}^{n},[27] where n is the total number of d + π^*(NO) electrons. Complex **2** and SOR would thus both be described as {FeNO}^{7} compounds, wherein the charge distribution could fall anywhere within the range Fe(I)−NO$^+$, to Fe(II)−NO$^\bullet$, to Fe(III)−NO$^-$.[18,27] In order to accurately assess the most appropriate electronic description, detailed spectroscopic (Mossbauer, MCD, EPR, X-ray absorption spectroscopy (XAS), IR, and/or resonance Raman) and theoretical (DFT) studies would be required.[8,11,14,28−33] Complex **6**,[26] on the other hand, would be described as an {FeNO}^{6} compound, wherein the charge distribution could fall anywhere within the range Fe(II)−NO$^+$, to Fe(III)−NO$^\bullet$, to Fe(IV)−NO$^-$. Complex **2** is irreversibly oxidized at a potential of E_{pa} = +450 mV (vs SCE) in MeCN solution (Figure S-2, Supporting Information), implying that its {FeNO}^{6} derivative is unstable in this solvent.

Nitric oxide-induced bond length changes in **2** are caused by several factors, including an increase in both coordination number and oxidation state (*vide infra*) and the introduction of a strong-field ligand. The Fe−N(3,3′) bonds elongate (by 0.074 Å), whereas the Fe−S(1) and Fe−N(2) bond lengths decrease (by 0.050 and 0.057 Å, respectively). The increase in Fe−N(3,3′) bond lengths is most likely caused by the increase in coordination number and steric crowding in the FeN(1)N(3)N(3′)N(4) plane which results from the introduction of the NO ligand. For the ligating atoms, S(1) and N(2), orthogonal to this plane, bond length decreases are observed, most likely due to an increase in Z_{eff} (*vide infra*)[31] and oxidation state, resulting from the oxidative addition of NO, and the absence of the steric factors present in the FeN(1)N(3)N(3′)N(4) plane. Although one would expect the *trans* influence of the NO ligand to elongate the Fe−N(1) bond, there is very little change to this bond length (less than 3 esd's), most likely because the metal ion oxidation state increase (*vide infra*) offsets the *trans* influence. Being *trans* to the NO ligand, the imine nitrogen N(1) is less affected by steric crowding. The extremely short Fe−X (X = NO) bond of **2** (Table 2) reflects the highly covalent nature of the Fe−NO bond.[18,27] This bond length is comparable to the DFT-calculated distance in IPNS Fe−NO,[16] slightly above the range typical for {FeNO}^{7} species (1.68−1.76 Å), and well above that of {FeNO}^{6} species (1.63−1.67 Å),[18,28,32,34−40] including $[Fe(S_2{}^{Me_2}N_3(Pr,Pr))(NO)]^+$ (**6**, Fe−NO = 1.676(3) Å).[26] The N−O bond length (1.118(6) Å) in **2** is closer to that of free NO (1.15 Å) than to NO$^-$ (1.26 Å) and is unexpectedly shorter than that of **6** (1.161(4) Å), despite the presence of an additional electron in the π^*-manifold of {FeNO}^{7} **2** versus {FeNO}^{6} **6**. Although the *trans* thiolate (present in **6**, but not in **2**) could be responsible for the longer N−O bond in **6**,[19] it might also simply be an artifact of disorder. The nitric oxide oxygen (O(1)) is disordered over two positions in structure **2** (but not in **6**), making the N−O bond distance a less reliable parameter (in **2**).

Vibrational Data. The solid-state (KBr pellet) IR spectrum of the NO-bound product, $[Fe(S^{Me_2}N_4(tren)(NO)]^+$ (**2**), displays an ^{15}NO isotope-sensitive stretch at $\nu_{NO}(\nu_{15}NO)$ = 1685(1640) cm^{-1} (Figure S-3, Supporting Information). This frequency is substantially shifted below that of free NO$^\bullet$ (ν_{NO} = 1875 cm^{-1}) and closer to that of free NO$^-$ (ν_{NO} = 1470 cm^{-1}),[18] consistent with the *oxidative addition* of NO to the metal ion and activation of the N−O bond. Spectroscopic and theoretical data indicate that NO is also reduced and activated upon binding to the Fe^{2+} sites of SOR,[8] isopenicillin N-synthase (IPNS),[16] and superoxide dismutase (SOD).[30] The ν_{NO} frequency of **2** is, however, significantly lower than that of NO-bound SOR ($\nu_{NO}(\nu_{15}NO)$ = 1721(1690) cm^{-1}),[8] indicating that more electron density shifts from the Fe^{2+} ion to the NO in **2**. Vibrational data are not available for NO-bound IPNS and SOD. One would expect the ν_{NO} stretching frequency to reflect the amount of electron density in the π^*(NO) and/or σ^*(NO) orbitals, which would be affected by the total number of d + π^*(NO) electrons, the ligand field of the metal ion, and the charge distribution within the Fe−NO bond. The ν_{NO} stretch of **2** falls in the range (1607−1812 cm^{-1})[18,28] typically observed for non-heme {FeNO}^{7} compounds[27] and is closest to those shown to possess an Fe(II)−NO$^\bullet$ (ν_{NO} = 1607−1682 cm^{-1}),[18,28,35,37,41−43] as opposed to an Fe(III)−NO$^-$ (ν_{NO} = 1710−1812 cm^{-1}),[11,18,29,44] electronic structure. Compounds with the Fe(III)−NO$^-$ electron distribution are S = 3/2 and have been shown, via detailed spectroscopic and theoretical calculations, to contain high-spin (S = 5/2) Fe(III) antiferromagnetically coupled to S = 1 NO$^-$.[8,11,30,33] In contrast, compounds with the Fe(II)−NO$^\bullet$ electron distribution are typically S = 1/2 and are usually described as containing a low-spin (S = 0) Fe(II) ligated by (S = 1/2) NO$^\bullet$,[28,29,32,45] although the electronic description of these compounds is more controversial.[31] Compound **2** is intermediate-spin S = 3/2 (*vide infra*), suggesting that the former description might be more accurate, despite the fact that the ν_{NO} frequency falls below that of an Fe(III)−NO$^-$ compound. Although counterintuitive, the higher ν_{NO} frequency for Fe(III)−NO$^-$ compounds is a result of the shift of π^* electron density away from the N−O bond and into the Fe−NO bond via constructive bonding overlap with the

half-filled Fe d_{xz} and d_{yz} orbitals.[46] As described previously,[8] one of these metal ion orbitals is filled in low-spin Fe(II), causing electron density to shift away from the Fe−NO bond and into the π^* N−O orbital in Fe(II)−$NO^{\bullet}$ compounds. DFT calculations show[31] that the electron-donating properties of the thiolate ligand of **2** have a similar effect by pushing electron density onto the metal ion, thereby preventing the shift of electron density away from the π^* N−O orbital and into the Fe−NO bond. This would imply that the thiolate ligand is responsible for the unusually low ν_{NO} frequency of **2** (1685 cm^{-1}). In support of this, nitrogen- and oxygen-ligated S = 3/2 Fe(III)−NO^- compounds, such as (TACN)Fe(NO)$(N_3)_2$,[11] (EDTA)Fe(NO),[11] $[Fe(NO)(^{iPr_3}tcmba)]^-$,[44] and $[Fe_2(NO)_2$-(Et-HPTB)$(O_2CPh)]^{2+}$,[47] for example, display ν_{NO} stretches at 1712, 1776, 1729, and 1785 cm^{-1}, respectively, whereas the ν_{NO} stretch (1682 cm^{-1}) for thiolate-ligated (TACN-$(BzS)_2$)Fe−NO[37] lies much closer to that of **2**. Given that the molecular charge and, in some cases, the coordination numbers of these compounds differ from those of **2**, these comparisons are not necessarily ideal. However, density functional calculations show that the ligand field and electron-donating properties of the thiolate ligand of **2** raise the energy of the d-orbitals relative to the π^* N−O, making it more energetically favorable for electrons to reside on the NO ligand in an antibonding orbital.[31] Together these data *imply that thiolate ligands promote more N−O bond activation in nitric oxide* than nitrogen- or oxygen-containing ligands *due to their electron-rich nature*. Hydrogen bonds attenuate the electron-donating properties of the SOR cysteinate ligand,[48,49] and this diminishes the extent of N−O bond activation by SOR, as is reflected in the higher ν_{NO} stretch (1721 cm^{-1}) for SOR−NO.[8] In contrast, RS···H bonds have been shown to strengthen the SOR Fe−O(peroxo) bond without influencing the peroxo O−O bond.[50] Most likely this is because a peroxo has two additional antibonding π^*(O−O) electrons relative to an NO ligand, making it a poorer electron acceptor. This prevents the delocalization of electrons, at least via a mechanism involving π-overlap, and decreases the covalency of the Fe−OOH bond relative to an Fe−NO bond.[8]

Electronic and Magnetic Properties of $[Fe(S^{Me_2}N_4(tren))(NO)]^+$ (2). Both the temperature-dependent magnetic susceptibility curve for solid samples of **2** (Figure S-4, Supporting Information, μ_{eff} = 4.12 μ_B) and the near-ambient temperature (290 K) solution-state magnetic moment of **2** (μ_{eff} = 3.95 μ_B in MeCN) are consistent with an S = 3/2 ground state that is maintained over a wide tempertaure range (5−290 K). The low-temperature (6.3 K) X-band EPR spectrum of **2** is rhombic, with features at g_x = 4.44, g_y = 3.54, and g_z = 1.97 (Figure 2), also consistent with an S = 3/2 spin state. Shoulders on the g = 4.44, 3.54 features could be attributed to either the superhyperfine interaction between the unpaired electron spin and the ^{14}N (I = 1) nucleus of the NO ligand[32] or to slightly different conformations of the molecule. The anisotropic nature of this spectrum indicates that the metal ion has been oxidized as a result of NO addition. Nitric oxide-bound SOR[17] and IPNS[14] are also intermediate-spin S = 3/2 and display rhombic EPR signals with features at g = 4.34, 3.76, 2.00 and g = 4.09, 3.95, 2.0, respectively, also consistent with oxidative NO addition. The former contains a thiolate sulfur *trans* to the NO, whereas the latter contains a thiolate sulfur *cis* to the NO, showing that the S = 3/2 ground state is favored regardless of the orientation of the thiolate ligand.

As mentioned earlier, nitric oxide-bound complexes and enzymes belonging to the $\{FeNO\}^7$ class can be either low-spin (S = 1/2)[28,35,37,41−43] or intermediate-spin (S = 3/2),[11,12,29,44,51] depending on the ligand environment.[18] The ν_{NO} frequency for

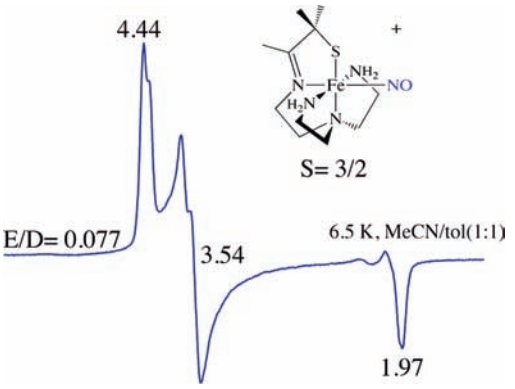

Figure 2. Low-temperature (6.5 K) X-band EPR of $[Fe(S^{Me_2}N_4(tren)$-(NO)][OTf] (**2**) in MeCN/toluene (1:1) glass.

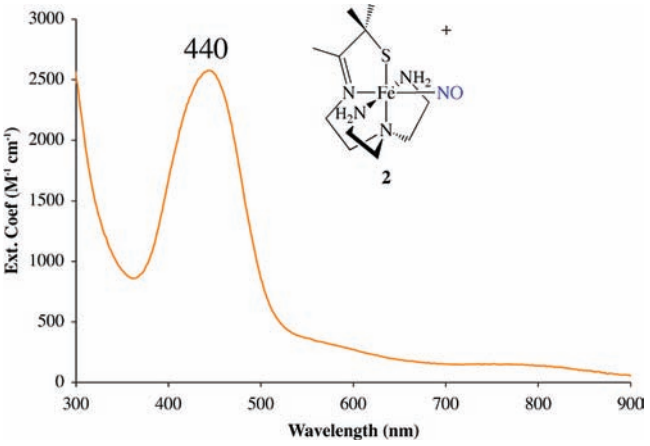

Figure 3. Electronic absorption spectrum of **2** in MeCN (298 K).

S = 3/2 Fe(III)−NO^- compounds tends to be higher than for S = 1/2 Fe(II)−$NO^{\bullet}$ compounds. Although the ν_{NO} stretching frequency of **2** falls in the range typically seen with Fe(II)−$NO^{\bullet}$ compounds, the S = 3/2 spin state would be inconsistent with this electronic structure and suggests that it is better described as containing a high-spin (S = 5/2) Fe^{III} antiferromagnetically coupled to NO^- (S = 1).[11] DFT calculations support this description.[31] The electronic absorption spectrum of **2**, which displays an intense band at λ = 440(2560) nm in MeCN (Figure 3), is also more consistent with this electronic description. Intense bands in this energy region are a characteristic feature of S = 3/2 Fe^{III}−NO^- systems, have been assigned as $NO^-(\pi^*)\rightarrow Fe^{3+}(d\pi)$ charge-transfer transitions,[11,16,33,44] and reflect the highly covalent nature of the Fe−NO bond. An analogous, albeit weaker, band is seen in the red-brown NO-bound form of SOR at 475(530) nm.[17]

In addition to the EPR and electronic absorption spectral data described above, recently obtained sulfur K-edge X-ray absorption spectral (XAS) data and DFT calculations[31] also support an Fe^{III}−NO^- electronic description for **2**. Two intense pre-edge features (at 2470.1 and 2571.0 eV)[31] are seen in the sulfur K-edge XAS spectrum of **2**, which can be assigned as sulfur 1s-to-metal ion 3d transitions. These transitions are in the region typically observed for thiolate-ligated Fe(III) complexes and reflect the effective nuclear charge (Z_{eff}) at the metal ion, and thus the oxidation state. On the basis of the energy of these transitions, the iron oxidation state in complex **2** is estimated (using Slater−Zener rules)[31] to be $Fe^{+2.75}$.

dx.doi.org/10.1021/ja107551u |*J. Am. Chem. Soc.* 2011, 133, 1419–1427

Scheme 3

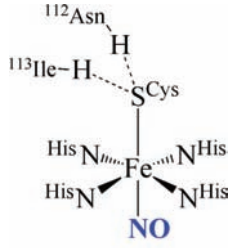

SOR–NO

The minimized DFT structure and calculated MO diagram show that the ligand field of **2** favors an $S = 5/2$ spin state, and calculated Mulliken spin densities show that the $S = 5/2$ Fe(III) and $S = 1$ NO^- are antiferromagnetically coupled.[31] Delocalization of electrons from the NO^- to the Fe d-orbitals slightly decreases the Z_{eff} and thus the oxidation state from Fe^{3+} to $Fe^{+2.75}$.[31] Thus, sulfur K-edge XAS data and DFT calculations for **2** are most consistent with an electronic structure consisting of a high-spin ($S = 5/2$) Fe^{III} antiferromagnetically coupled to NO^- ($S = 1$).[31] The electronic structure of nitric oxide-bound SOR has also been shown to be best described in the same manner.[17]

Relevance to SOR. Nitric oxide binding to **1** probes the superoxide binding site of our biomimetic SOR analogue.[1,9] The associated structural changes, as well as the vibrational ν_{NO} parameter, electronic absorption data, DFT calculations,[31] and sulfur K-edge XAS data[31] for NO-bound **2**, are consistent with a mechanism involving the *oxidative addition* of NO (and thus superoxide) *cis* to the thiolate. A similar oxidative mechanism is involved in NO binding to SOR, except that NO binds *trans*, as opposed to *cis*, to the thiolate.[17] To our knowledge, **2** is the first reported synthetic analogue of SOR-NO. Additional parallels can be drawn between NO-bound **2** and SOR-NO, including an identical $S = 3/2$ spin state and similar EPR and electronic absorption spectra. Given the *trans* influence of thiolates and the push/pull effect of combining a π-donating thiolate with a π-accepting NO, one might expect *trans*-cysteinate-ligated SOR-NO ($\nu_{NO} = 1721\ cm^{-1}$)[8] to have a lower, rather than higher, ν_{NO} frequency relative to *cis*-thiolate-ligated **2** ($\nu_{NO} = 1685\ cm^{-1}$). However, hydrogen-bonding between the cysteinate sulfur and two highly conserved SOR residues (Scheme 3) causes the thiolate sulfur to donate less electron density to the NO (via the metal ion) in SOR, thereby increasing its ν_{NO} stretching frequency.[48] Similar effects have been noted with synthetic H-bonded thiolate/porphyrin-ligated ferric compounds.[19] Hydrogen-bonding noticeably lengthens the SOR Fe–S^{cys} bond (to 2.46 Å)[48] and has also been suggested to modulate reactivity.[49,50] Together these data would imply that electron density at the thiolate sulfur and its overlap with a metal ion orbital that is involved in bonding to NO are more important than the thiolate's *trans* influence in determining the extent of N–O bond activation. With P450, a *trans* orientation of the cysteinate ligand is proposed to promote O–O, as opposed to Fe–O bond cleavage, due to its *trans* effect (the "push effect") and the low-spin-state-induced strengthening of the Fe–O bond.[52,53] In contrast, Goldberg and Niviere have each concluded that *trans* thiolate donors weaken peroxo Fe–O bonds (in SOR[50] and related model complexes)[3] without affecting O–O bond strengths, even with a low-spin peroxo. Recent DFT calculations suggest that a spin-crossing barrier would prevent H_2O_2 release from the low-spin

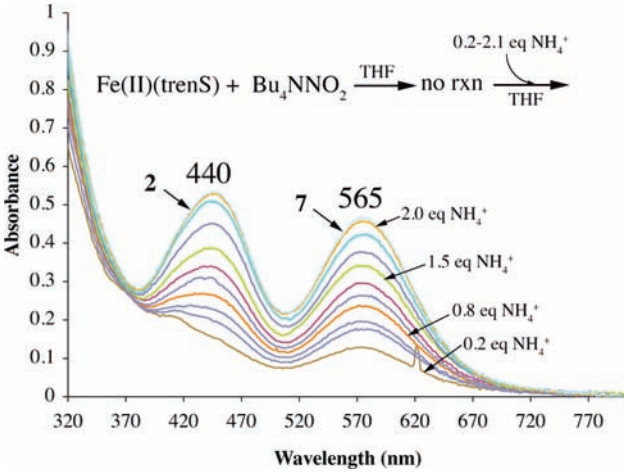

Figure 4. Reaction between colorless [Fe($S^{Me_2}N_4$(tren)][OTf] (**1**) and 1 equiv of NO_2^- in THF (298 K) requires 2 equiv of proton donor (NH_4^+) and affords two intensely colored products, **2** and **7**.

Scheme 4

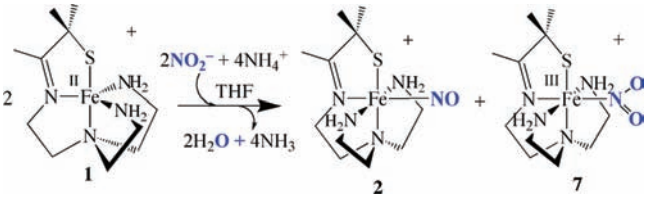

Fe–OOH of P450.[49] However, low-spin ($S = 1/2$) [Fe^{III}($S^{Me_2}N_4$(tren))(OOH)]$^+$ has been shown to release H_2O_2 via a proton-induced mechanism.[1,54] NO-bound {FeNO}^{7} **2**, described herein, provides a less reduced analogue of metastable {FeOOH}^{9} [Fe^{III}($S^{Me_2}N_4$(tren))(OOH)]$^+$. Given the π-accepting properties of NO (and not HOO^-), it is not surprising that the factors which affect thiolate-induced Fe–NO vs N–O bond activation are different from those which would affect Fe–O vs O–O bond activation in iron peroxos. With **2**, we were not able to detect any ν_{Fe-NO} stretches for **2** and thereby assess anything about its Fe–NO bond strength relative to other {FeNO}^{7} complexes lacking a thiolate ligand.

Proton-Dependent Reduction of Nitrite. In order to determine whether thiolate-ligated [Fe^{II}($S^{Me_2}N_4$(tren))]$^+$ (**1**) is capable of reducing substrates other than superoxide and nitric oxide, we also examined its reactivity with nitrite (NO_2^-). Nitrite is a biologically relevant[55–57] π-acceptor ligand, which has been shown to form strong bonds to heme and non-heme Fe(II).[58,59] If 1 equiv of Bu_4NNO_2 is added to colorless **1** in THF, no observable reaction occurs (as monitored by electronic absorption spectroscopy) until an external proton donor (such as NH_4^+) is added, indicating that the reaction is proton-dependent. Two equivalents of proton donor are required per equivalent of NO_2^- (Figure 4), and two products are observed in a 1:1 ratio (Scheme 4), each of which was identified via independent synthesis and structural characterization. One of the products, nitrite-bound [Fe^{III}($S^{Me_2}N_4$(tren))(NO_2)]$^+$ (**7**) ($\lambda_{max} = 565(1458)$ nm; Figure S-5, Supporting Information), can be synthesized directly (*vide infra*) via the addition of 1 equiv of NO_2^- to [Fe^{III}($S^{Me_2}N_4$(tren))(MeCN)]$^{2+}$ (**8**). The other product, [Fe($S^{Me_2}N_4$(tren)(NO)]$^+$ (**2**) (*vide supra*, $\lambda_{max} = 440(2560)$ nm), contains a two-electron-reduced NO^- ligand

dx.doi.org/10.1021/ja107551u | J. Am. Chem. Soc. 2011, 133, 1419–1427

Scheme 5

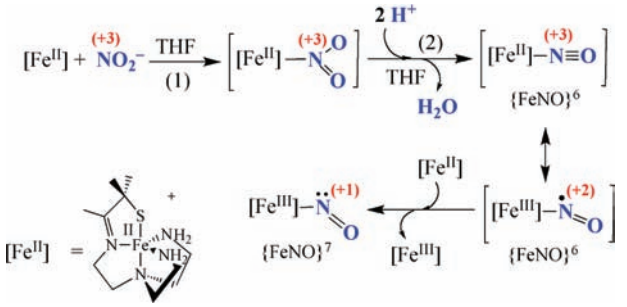

(Scheme 5, eq 1). The rate of this reaction was found to depend on the pK_a of the proton donor, taking 3 h (with 0.75 mM of **1** and 1.02 mM Bu_4NNO_2) to go to completion in MeOH, versus 3 min (with 0.56 mM of **1** and 0.78 mM Bu_4NNO_2) in THF with added NH_4^+. Quantitative titrations monitored via electronic absorption spectroscopy (Figure S-6, Supporting Information) establish that two equivalents of Fe(II) are consumed per equivalent of NO_2^- reduced (to afford Fe(III)−NO^- (**2**)). The other equivalent of NO_2^- binds to the oxidized $[Fe^{II}(S^{Me_2}N_4(tren))]^+$ electron donor to afford **7** (Scheme 4). If a sacrificial reductant, such as $NaBH_4$, is added, then only one equivalent of Fe(II) is required per equivalent of NO_2^- reduced, and only one Fe-containing product, $[Fe(S^{Me_2}N_4(tren)(NO)]^+$ (**2**), forms (Figure S-7, Supporting Information). Although no intermediates are detected in this reaction, even at temperatures as low as −78 °C (Figure S-7), likely intermediates would include nitrite-bound ferrous $[Fe^{II}(S^{Me_2}N_4(tren))(NO_2)]$ (**9**; step (1) of Scheme 5), if the reaction occurs via an inner-sphere mechanism similar to that of **1**-promoted O_2^- reduction.[1,9,54] An Fe^{II}−NO_2^- intermediate is implicated in the mechanism of heme iron-containing nitrite reductase (NiR)-promoted NO_2^- reduction,[55] and related synthetic porphyrin-ligated Fe^{II}−NO_2^- compounds have been isolated.[58] Extensive π-back-bonding within the Fe^{II}−NO_2^- fragment is proposed to facilitate heterolytic N−O bond cleavage by NiR.[55] Proton-induced heterolytic cleavage of the N−O bond (step (2) of Scheme 5) would initially convert proposed nitrite-bound intermediate $[Fe^{II}(S^{Me_2}N_4(tren))(NO_2)]$ (**9**) to $[Fe(S^{Me_2}N_4(tren)(NO)]^{2+}$ (**10**), the less stable, oxidized $\{FeNO\}^6$ derivative of **2** (*vide supra*). An $\{FeNO\}^6$ species would contain nitrogen in either a +3 (Fe(II)−NO^+) or +2 (Fe(III)−$NO^\bullet$) oxidation state, meaning that N−O bond cleavage may or may not be reductive in this first N−O bond-cleaving step (step (2) of Scheme 5). The necessity for two protons, as opposed to one proton, implies that H_2O, as opposed to OH^-, is the preferred leaving group, as one would expect in THF solvent. A thiolate would help promote this step either by activating the N−O bond via the transfer of electron density into the π^*(N−O) and/or σ^*(N−O) orbital(s) or by favoring the formation of a highly covalent Fe(III)−SR bond. It would also facilitate proton-induced heterolytic N−O bond cleavage by making the nitrite oxygen more basic. Thiols have previously been shown to reduce Fe(III)−NO_2^- species to afford an $\{FeNO\}^7$ product.[60] Both $\{FeNO\}^6$ and $\{FeNO\}^7$ species have been implicated as intermediates in NiR-promoted NO_2^- reduction, although these have proven difficult to detect.[55,61] Consistent with its limited stability (*vide supra*), an intermediate $\{FeNO\}^6$ species, $[Fe(S^{Me_2}N_4(tren)(NO)]^{2+}$ (**10**), is not observed in NO_2^- reduction by **1**. Instead, a second equivalent of Fe(II) is consumed (step (3) of Scheme 5) in order to afford the more stable $\{FeNO\}^7$

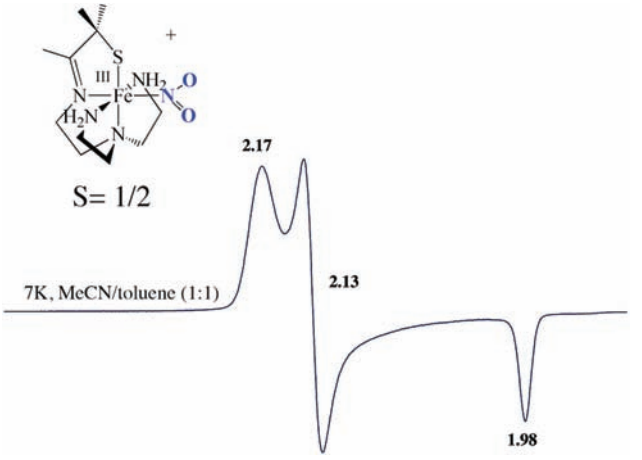

Figure 5. Low-temperature (7 K) X-band EPR spectrum of $[Fe^{III}(S^{Me_2}N_4(tren))(NO_2)]^+$ (**7**) in MeCN/toluene (1:1) glass.

Scheme 6

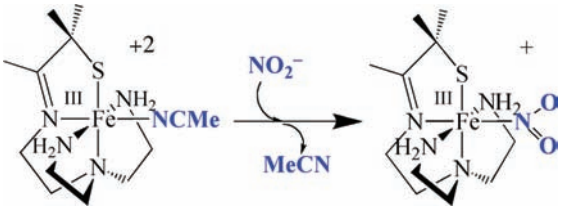

species **2**. Thus, the net reaction promoted by **1** is the two-electron, two-proton reduction of nitrite to the nitric oxide anion NO^- (eq 1).

$$NO_2^- + 2e^- + 2H^+ \rightarrow NO^- + H_2O \qquad (1)$$

The proton dependence of NO_2^- reduction by **1** is similar to that of superoxide reduction by **1**. Recent kinetics studies showed that initial protonation of the superoxide anion (O_2^-) is necessary in order to generate a more potent HO_2 oxidant.[54] With NO_2^- reduction (Scheme 5), protons are most likely required in order to promote heterolytic (as opposed to homolytic) cleavage of the N−O bond.[55] Given the instability of O^{2-}, heterolytic N−O bond cleavage is unlikely to occur in the absence of protons. The pH-dependent redox potential of NO_2^- ($E_{1/2}$(pH 14) = −0.46 V; $E_{1/2}$(pH 0) = +0.996 V vs NHE) and its relative position on the basic, versus acidic, Frost diagrams[62] support this and show that protons are essential in order to make NO_2^- reduction feasible under mild conditions.

Nitrite-bound $[Fe^{III}(S^{Me_2}N_4(tren))(NO_2)]^+$ (**7**; 1478 cm^{-1} ($\nu_{asym}(NO_2)$), 1362 cm^{-1} ($\nu_{sym}(NO_2)$)) was independently synthesized via the addition of 1 equiv of NO_2^- to $[Fe^{III}(S^{Me_2}N_4(tren))(MeCN)]^{2+}$ (**8**, Scheme 6) and crystallographically characterized. In protic solvents (e.g., MeOH), NO_2^--bound **7** can also be generated via O_2 oxidation of NO-bound **2** (Figure S-8, Supporting Information). In contrast to high-spin **2**, nitrite-bound **7**, which contains a more highly oxidized Fe^{3+} ion, is low-spin (g = 2.17, 2.13, 1.98 (Figure 5); μ_{eff}(MeCN, 303 K) = 1.76 μ_B; μ_{eff}(solid state) = 1.72 μ_B (Figure S-9, Supporting Information)), most likely due to the stronger, more covalent Fe(III)−SR bond (Table 2). As shown in the ORTEP diagram of Figure 6, nitrite coordinates to **7** as the more commonly observed η^1-N (nitro) (as opposed to η^1-O (nitrito)) linkage isomer,[63]

dx.doi.org/10.1021/ja107551u |*J. Am. Chem. Soc.* 2011, 133, 1419–1427

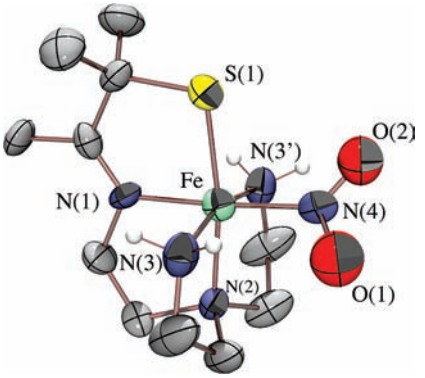

Figure 6. ORTEP plot of the cation of $[Fe^{III}(S^{Me_2}N_4(tren)(NO_2)](PF_6)$ (**7**). All H-atoms have been omitted for clarity.

with NO_2^- *trans* to the imine and *cis* to the thiolate. The Fe−S(1) bond of **7** is 0.1 Å shorter than that of nitric oxide-ligated **2** (Table 2) and is closer to that of authentic ferric complexes **3** and **4**, indicating that Z_{eff}, i.e., the metal ion oxidation state, is higher in **7** (+3) than in **2** (+2.75).[31]

Due to the less covalent nature of the iron−nitrogen bond, the Fe−N(4) distance is 0.193 Å longer in NO_2-bound **7** versus NO-bound **2**. The Fe−N(4)−O bond angle is closer to that of an idealized sp^2-hybridized nitrogen N(4) in **7** (123.9(9)°) versus **2** (151.7(4)°).

SUMMARY AND CONCLUSIONS

In order to probe the superoxide (O_2^-) and dioxygen (O_2) binding site of our thiolate-ligated biomimetic SOR model $[Fe^{II}(S^{Me_2}N_4(tren))]^+$ (**1**) and gain insight regarding the mechanism of N−O (and thus O−O) bond activation, a nitric oxide (NO)-bound derivative $[Fe(S^{Me_2}N_4(tren)(NO)]^+$ (**2**) was synthesized and spectroscopically characterized. The *electron-rich thiolate ligand was found to enhance N−O bond activation*, resulting in an unusually low ν_{NO} frequency. Structural, magnetic, and spectroscopic (UV/vis, IR) data were all found to be consistent with a *mechanism* involving the *oxidative addition of NO* to **1** and an electronic description for $S = 3/2$ $\{FeNO\}^7$ **2** consisting of a high-spin ($S = 5/2$) Fe(III) antiferromagnetically coupled to NO^- ($S = 1$). Recent sulfur K-edge XAS data and DFT calculations support this.[31] Comparison of the properties of NO-bound **2** with those of NO-bound SOR shows that, while the $S = 3/2$ spin state is identical and the EPR and electronic absorption spectra are similar, the ν_{NO} frequency is considerably lower in **2**, despite the presence of a *cis*, as opposed to *trans*, thiolate. Hydrogen-bonding to the cysteinate is suggested to be responsible for attenuating the extent of N−O bond activation in SOR by decreasing the sulfur ligand's electron-donating properties. In contrast, the ν_{O-O} frequency of SOR peroxo intermediate and its analogues[3] is not affected by H-bonds to the cysteinate sulfur[50] or other factors influencing the Fe−SR bond strength. These only influence the ν_{Fe-O} frequency. Given that a peroxo ligand has two additional antibonding π^*(O−O) electrons relative to an NO ligand, it cannot π-accept electron density and therefore has a less covalent Fe−X (X = OOH, NO) bond relative to an Fe−NO compound. Thiolate-ligated **1** was also shown to *promote the proton-dependent heterolytic cleavage of an N−O bond of nitrite* (NO_2^-) to afford NO^--bound **2**, the overall reaction of which was shown to involve the $2e^-/2H^+$ reduction of NO_2^-. The mechanism of this reaction is proposed to involve both nitrite-bound ferrous $[Fe^{II}(S^{Me_2}N_4(tren))(NO_2)]$ and $\{FeNO\}^6$ intermediates similar to those implicated in the mechanism of nitrite reductase-promoted NO_2^- reduction.[55]

ASSOCIATED CONTENT

Supporting Information. Experimental and crystallographic data for complexes **2** and **7**, including an ESI mass spectrum, cyclic voltammogram, and IR spectrum of **2**; electronic absorption spectrum of **7**; magnetic data for **2** and **7**; and quantitative titrations and/or reactions between **1** and NO_2^-, and **2** and O_2, monitored by electronic absorption spectroscopy. This material is available free of charge via the Internet at http://pubs.acs.org.

AUTHOR INFORMATION

Corresponding Author
kovacs@chem.washington.edu

ACKNOWLEDGMENT

This work was supported by the NIH (GM 45881). We thank Morgan Gleaves and Jessica Pikul for experimental assistance. J.B., J.F., and W.K. are UW staff crystallographers.

REFERENCES

(1) Shearer, J.; Scarrow, R. C.; Kovacs, J. A. *J. Am. Chem. Soc.* **2002,** *124*, 11709–11717.
(2) Kitagawa, T.; Dey, A.; Lugo-Mas, P.; Benedict, J.; Kaminsky, W.; Solomon, E.; Kovacs, J. A. *J. Am. Chem. Soc.* **2006,** *128*, 14448–14449.
(3) Namuswe, F.; Kasper, G. D.; Narducci Sarjeant, A. A.; Hayashi, T.; Krest, C. M.; Green, M. T.; Moenne-Loccoz, P.; Goldberg, D. P. *J. Am. Chem. Soc.* **2008,** *130*, 14189–14200.
(4) Bukowski, M. R.; Halfen, H. L.; van der Berg, T. A.; Halfen, J. A.; Que, L., Jr. *Angew. Chem., Int. Ed.* **2005,** *44*, 584–587.
(5) Krishnamurthy, D.; Kasper, G. D.; Namuswe, F.; Kerber, W. D.; Sarjeant, A. N.; Moënne-Loccoz, P.; Goldberg, D. P. *J. Am. Chem. Soc.* **2006,** *128*, 14222–14223.
(6) Jiang, Y.; Telser, J.; Goldberg, D. P. *Chem. Commun.* **2009,** 6828–6830.
(7) Clay, M. D.; Jenney, F. E., Jr.; Hagedoorn, P. L.; George, G. N.; Adams, M. W. W.; Johnson, M. K. *J. Am. Chem. Soc.* **2002,** *124*, 788–805.
(8) Clay, M. D.; Cosper, C. A.; Jenney, F. E.; Adams, M. W.; Johnson, M. K. *Proc. Natl. Acad. Sci. U.S.A.* **2003,** *100*, 3796–3801.
(9) Shearer, J.; Nehring, J.; Kaminsky, W.; Kovacs, J. A. *Inorg. Chem.* **2001,** *40*, 5483–5484.
(10) Theisen, R. M.; Shearer, J.; Kaminsky, W.; Kovacs, J. A. *Inorg. Chem.* **2004,** *43*, 7682–7690.
(11) Brown, C. A.; Pavlosky, M. A.; Westre, T. E.; Zhang, Y.; Hedman, B.; Hodgson, K. O.; Solomon, E. I. *J. Am. Chem. Soc.* **1995,** *117*, 715–732.
(12) Nelson, M. J. *J. Biol. Chem.* **1987,** *262*, 12137–12142.
(13) Wolfe, M. D.; Parales, J. V.; Gibson, D. T.; Lipscomb, J. D. *J. Biol. Chem.* **2001,** *276*, 1945–1953.
(14) Chen, V. J.; Orville, A. M.; Harpel, M. R.; Frolic, C. A.; Suresus, K. K.; Münck, E.; Lipscomb, D. J. *J. Biol. Chem.* **1989,** *264*, 21677–21681.
(15) Roach, P. L.; Clifton, I. J.; Hensgens, C. M. H.; Shibita, N.; Shofield, C. J.; Hajdu, J.; Baldwin, J. E. *Nature* **1997,** *387*, 827–830.
(16) Brown, C. D.; Neidig, M. L.; Neibergall, M. B.; Lipscomb, J. D.; Solomon, E. I. *J. Am. Chem. Soc.* **2007,** *129*, 7427–7438.
(17) Clay, M.; Cosper, C. A.; Jenney, F. E., Jr.; Adams, M. W. W.; Johnson, M. K. *Proc. Natl. Acad. Sci. U.S.A.* **2003,** *100*, 3796–3801.
(18) McCleverty, J. A. *Chem. Rev.* **2004,** *104*, 403–418.
(19) Paulat, F.; Lehnert, N. *Inorg. Chem.* **2007,** *46*, 1547–1549.

(20) Ellison, J. J.; Nienstedt, A.; Shoner, S. C.; Barnhart, D.; Cowen, J. A.; Kovacs, J. A. *J. Am. Chem. Soc.* **1998,** *120*, 5691–5700.
(21) Evans, D. A. *J. Chem. Soc.* **1959,** 2005.
(22) Live, D. H.; Chan, S. I. *Anal. Chem.* **1970,** *42*, 791.
(23) Van Geet, A. L. *Anal. Chem.* **1968,** *40*, 2227–2229.
(24) Shearer, J.; Fitch, S. B.; Kaminsky, W.; Benedict, J.; Scarrow, R. C.; Kovacs, J. A. *Proc. Natl. Acad. Sci. U.S.A.* **2003,** *100*, 3671–3676.
(25) Conradie, J.; Hopmann, K. H.; Ghosh, A. *J. Phys. Chem. B* **2010,** *114*, 8517–8524.
(26) Schweitzer, D.; Ellison, J. J.; Shoner, S. C.; Lovell, S.; Kovacs, J. A. *J. Am. Chem. Soc.* **1998,** *120*, 10996–10997.
(27) Enemark, J. H.; Feltham, R. D. *Coord. Chem. Rev.* **1974,** *13*, 339–406.
(28) Serres, R. G.; Grapperhaus, C. A.; Bothe, E.; Bill, E.; Weyhermuller, T.; Neese, F.; Wieghardt, K. *J. Am. Chem. Soc.* **2004,** *126*, 5138–5153.
(29) Hauser, C.; Glaser, T.; Bill, E.; Weyhermuller, T.; Wieghardt, K. *J. Am. Chem. Soc.* **2000,** *122*, 4352–4365.
(30) Jackson, T. A.; Yikilmaz, E.; Miller, A. F.; Brunold, T. C. *J. Am. Chem. Soc.* **2003,** *125*, 8348–8363.
(31) Sun, N.; Dey, A.; Villar-Acevedo, G.; Kovacs, J. A.; Darensbourg, M. Y.; Hodgson, K. O.; Hedman, B.; Solomon, E. *Inorg. Chem.* **2011,** *50*, 427–436.
(32) Ghosh, P.; Stobie, K.; Bill, E.; Bothe, E.; Weyhermuller, T.; Ward, M. D.; McCleverty, J. A.; Wieghardt, K. *Inorg. Chem.* **2007,** *46*, 522–532.
(33) Zhang, Y.; Pavlosky, M. A.; Brown, C. A.; Westre, T. E.; Hedman, B.; Hodgson, K. O.; Solomon, E. I. *J. Am. Chem. Soc.* **1992,** *114*, 9189–9191.
(34) Xu, N.; Powell, D. R.; Cheng, L.; Richter-Addo, G. B. *Chem. Commun. (Cambridge)* **2006,** 2030–2032.
(35) Harrop, T. C.; Olmstead, M. M.; Mascharak, P. K. *Inorg. Chem.* **2005,** *44*, 6918–6920.
(36) Afshar, R. K.; Patra, A. K.; Olmstead, M. M.; Mascharak, P. K. *Inorg. Chem.* **2004,** *43*, 5736–5743.
(37) Li, M.; Bonnet, D.; Bill, E.; Neese, F.; Weyhermuller, T.; Blum, N.; Sellmann, D.; Wieghardt, K. *Inorg. Chem.* **2002,** *41*, 3444–3456.
(38) Sellmann, D.; Blum, N.; Heinemann, F. W.; Hess, B. A. *Chem.—Eur. J.* **2001,** *7*, 1874–1880.
(39) Lupez, J. P.; Heinemann, F. W.; Prakash, R.; Hess, B. A.; Horner, O.; Jeandey, C.; Oddou, J.-L.; Latour, J.-M.; Grohmann, A. *Chem.—Eur. J.* **2002,** *8*, 5709–5722.
(40) Scheidt, W. R.; Lee, Y. J.; Hatano, K. *J. Am. Chem. Soc.* **1984,** *106*, 3191–3198.
(41) Karlin, K. D.; Rabinowitz, H. N.; Lewis, D. L.; Lippard, S. J. *Inorg. Chem.* **1977,** *16*, 3262–3267.
(42) Afshar, R. K.; Patra, A. K.; Bill, E.; Olmstead, M. M.; Mascharak, P. K. *Inorg. Chem.* **2006,** *45*, 3774–3781.
(43) Lopes, L. G. F.; Sousa, E. H. S.; Miranda, J. C. V.; Oliveira, C. P.; Caralho, I. M. M.; Batista, A. A.; Ellena, J.; Castellano, E. E.; Nascimento, O. R.; Moreira, I. S. *J. Chem. Soc., Dalton Trans.* **2002,** 1903–1906.
(44) Ray, M.; Golombek, A. P.; Hendrich, M. P.; Yap, G. P. A.; Liable-Sands, L. M.; Rheingold, A. L.; Borovik, A. S. *Inorg. Chem.* **1999,** *38*, 3110–3115.
(45) Pierce, B. S.; Gardner, J. D.; Bailey, L. J.; Brunold, T. C.; Fox, B. G. *Biochemistry* **2007,** *46*, 8569–8578.
(46) Linder, D. P.; Rodgers, K. R.; Banister, J.; Wyllie, G. R. A.; Ellison, M. K.; Scheidt, W. R. *J. Am. Chem. Soc.* **2004,** *126*, 14136–14148.
(47) Feig, A. L.; Bautista, M. T.; Lippard, S. J. *Inorg. Chem.* **1996,** *35*, 6892–6898.
(48) Yeh, A. P.; Hu, Y.; Jenney, F. E., Jr.; Adams, M. W. W.; Rees, D. C. *Biochemistry* **2000,** *39*, 2499–2508.
(49) Dey, A.; Jenney, F. E.; Adams, M. W.; Johnson, M. K.; Hodgson, K. O.; Hedman, B.; Solomon, E. I. *J. Am. Chem. Soc.* **2007,** *129*, 12418–12431.
(50) Mathé, C.; Weill, C. O.; Mattioli, T. A.; Berthomieu, C.; Houée-Levin, C.; Tremey, E.; Nivière, V. *J. Biol. Chem.* **2007,** *282*, 22207–22216.
(51) Arciero, D. M.; Lipscomb, J. D. *J. Biol. Chem.* **1986,** *261*, 2170–2178.
(52) Denisov, I. G.; Makris, T. M.; Sligar, S. G.; Schlichting, I. *Chem. Rev.* **2005,** *105*, 2253–2277.
(53) Mak, P. J.; Denisov, I. G.; Victoria, D.; Makris, T. M.; Deng, T.; Sligar, S. G.; Kincaid, J. R. *J. Am. Chem. Soc.* **2007,** *129*, 6382–6383.
(54) Nam, E.; Alokolaro, P. E.; Swartz, R. D.; Gleaves, M. C.; Pikul, J.; Kovacs, J. A. *Inorg. Chem.* **2011,** *50*, in press.
(55) Einsle, O.; Messerschmidt, A.; Huber, R.; Kroneck, P. M. H.; Neese, F. *J. Am. Chem. Soc.* **2002,** *124*, 11737–11745.
(56) Halfen, J. A.; Mahapatra, S.; Wilkinson, E. C.; Gengenbach, A. J.; Young, V. G.; Que, L., Jr.; Tolman, W. B. *J. Am. Chem. Soc.* **1996,** *118*, 763–776.
(57) Averill, B. A. *Chem. Rev.* **1996,** *96*, 2951–2964.
(58) Nasri, H.; Ellison, M. K.; Krebs, C.; Huynh, B. H.; Scheidt, W. R. *J. Am. Chem. Soc.* **2000,** *122*, 10795–10804.
(59) Nasri, H.; Wang, Y.; Huynh, B. H.; Scheidt, W. R. *J. Am. Chem. Soc.* **1991,** *113*, 717–719.
(60) Nasri, H.; Haller, K. J.; Wang, Y.; Huynh, B. H.; Scheidt, W. R. *Inorg. Chem.* **1992,** *31*, 3459–3467.
(61) Wang, Y.; Averill, B. A. *J. Am. Chem. Soc.* **1996,** *118*, 3972–3973.
(62) Shriver, D. F.; Atkins, P. *Inorganic Chemistry*, 4th ed.; Oxford University Press: Oxford, UK, 2006.
(63) Wyllie, G. R. A.; Scheidt, W. R. *Chem. Rev.* **2002,** *102*, 1067–1089.